Performance comparison of different SiPM arrays coupled to neutron-γ scintillators

Jessica Delgado[1,2,*], Felix Pino[1], Sandra Moretto[1,3], Daniele Corti[3], Alessandro Griggio[3], Lucio Pancheri[4,5], Daniela Fabris[3]

[1]*Department of Physics and Astronomy "Galileo Galilei", University of Padova, Italy*
[2]*Department of Physics and Earth Science, University of Ferrara, Italy*
[3]*INFN- Padova Section, Italy*
[4]*Department of Industrial Engineering, University of Trento, Italy*
[5]*INFN-TIFPA Trento Section, Italy*
(*) jessicadelgadoalvarez@gmail.com

***Abstract*— The market for SiPMs has grown rapidly in recent years, driven by their increasing use in applications such as medical imaging, nuclear and particle physics. Due to the growing demand, many manufacturers are now offering SiPMs, each of them with unique features and performance characteristics. As a result, it is essential to conduct comparative studies to evaluate and compare the performance of different SiPM arrays. Therefore, this work aims to compare the performance of assembled detectors based on two different SiPM arrays (AdvanSiD-NUV hybrid array ASD-NUV4S-P-4x4TD 17 mm x17 mm and the MPPC Hamamatsu S14161-6050HS-04 25 mm x 25 mm) coupled to two organic scintillators, a liquid scintillator EJ-309 (50 mm diameter x 50 mm thickness) and a plastic scintillator EJ-276G (25 mm diameter x 25 mm thickness). The assessment of the performance was made in terms of their energy resolution, time resolution, and capability to discriminate between γ-rays and fast neutrons. The outcomes show that the Hamamatsu SiPM array performs better for all of the characteristics studied, with the best configuration being when it was coupled to the EJ-309 liquid scintillator, obtaining the lowest energy and time resolutions, (0.108 ±0.004) and (0.599 ± 0.004) ns respectively, and the highest Figure of Merit (2.04 ± 0.01). A good Figure of Merit value that ensures an effective discrimination between fast neutrons and γ-rays.**

***Keywords*—SiPM-arrays, n/γ discrimination, neutron detection, scintillators.**

I. Introduction

THE rapid advancement of silicon photomultiplier (SiPM) technology has led to an opportunity to investigate the replacement of commonly used photomultipliers (PMTs) by SiPMs as light converters in various applications, particularly in radiation detectors to be coupled to scintillators. Silicon Photomultipliers are high-sensitivity, high-efficiency light sensors that detect light ranging from near ultraviolet to near-infrared. They are made up of a matrix of sensitive micro-cells that are all connected in parallel. Each micro-cell is a Geiger-Mode avalanche photo-diode that operates beyond the breakdown voltage and incorporates a resistor for passive quenching [1].

The wide variety of applications on SiPM-based detectors goes from high-energy physics, particle physics, medical imaging, astronomy, to hazard and threat detection, among others, making SiPMs an active research target. Some of the most interesting characteristics of SiPMs are high photon detection efficiency, high gain at low operating voltages, compactness, and insensitivity to magnetic fields [2]. It should also be noted that SiPMs' prices are declining even as their technological advancements are accelerating. However, the SiPMs have some properties that make precise electronic readout difficult. These include a longer single photon response duration and relatively higher noise contributions from dark pulses, and after-pulsing [3]. Where a dark pulse is the result of a thermally generated electron that initiates an avalanche in the high field region, while the after-pulsing is produced by the release of carries that are trapped in the silicon crystal, and a second avalanche is created in the same microcell, the occurrence of this effect depends on the pixel recovery time [4]. Nevertheless, despite the noise that comes with SiPMs, they have demonstrated amazing results in terms of sensitivity, efficiency, and particle discrimination.

Among the most common SiPM arrays on the market are: 1. Hamamatsu SiPM arrays, which are manufactured by one of the leading SiPM array manufacturers. Their arrays have a high photon detection efficiency, a fast-timing resolution, and a low dark count rate [5]. 2. SensL, another manufacturer that offers SiPM arrays with high photon detection efficiency and low cross-talk [4]. 3. KETEK SiPM arrays, which have a low dark count rate and a low probability of after-pulsing [6]. 4. AdvanSiD, a company that provides SiPM arrays with high gain and a low after-pulsing probability [7]. Given that each SiPM array manufacturer has distinct characteristics and performance parameters, the choice of SiPM array depends on the specific application and experimental conditions.

Different investigations have been going on in order to compare these distinct characteristics, for example in a work done by M. Grodzicka-Kobylka [8], a SensL and a Hamamatsu SiPM arrays were compared in terms of γ spectrometry, using three inorganic scintillators (LSO, BGO, and CsI:Tl). In that study, the energy resolution, linearity, and stability of the two

arrays were studied in function of the temperature and bias voltage applied. The results indicate that both SiPM arrays demonstrate satisfactory energy resolution and linearity, but the SensL array performed better at low temperatures.

Another important parameter to be studied is the discrimination performance when a SiPM array is coupled to a scintillator with n/γ-ray discrimination capability. It represents an important feature in different fields, such as radiation monitor applications [9] and homeland security for identifying SNM (Special Nuclear Materials) [10]. The PSD (Pulse Shape Discrimination) technique using SiPM arrays is a challenging task, mainly because it is based on the reconstruction of the time profile of the scintillation decay, and, it must be taken into account that the conversion of the light into charge in a SiPM does not occur in the same way as in a PMT. Nevertheless, from a previous work conducted by our group, we demonstrated the possibility of doing n/γ-ray discrimination using large-sized scintillators coupled to large area SiPM arrays [7]. In that case, three commercial scintillators were used (EJ-276, EJ-309, and EJ-301, with diameters ranging from 20 to 50 mm) in conjunction with two large areas of SiPM arrays from AdvanSiD (NUV and RGB). Good n/γ-ray discrimination was obtained for all combinations, with results comparable to the ones obtained using a PMT as a read-out. Taking these advancements into consideration, we continue our research, but this time using and compare different types of SiPM arrays.

In the current paper, we compare the performance of assembled detectors based on two organic scintillators with n/γ-ray discrimination capabilities, a plastic scintillator EJ-276G (25 mm dia. x 25 mm thick.) and a liquid scintillator EJ-309 (50 mm dia. x 50 mm thick.), both with cylindrical shape and from Eljen Technology–Texas USA, coupled to two different SiPM arrays, the AdvanSiD-NUV hybrid array ASD-NUV4S- P-4x4TD 17 mm x17 mm and the MPPC Hamamatsu S14161-6050HS-04 25 mm x25 mm. The performance was assessed in terms of the energy resolution, time resolution, and n/γ discrimination. The purpose of this work is to provide the performance characteristics of the four possible configurations in order to aid future studies toward a better selection of a SiPM array for a specific experiment or application.

II. Methods and Experimental Set-up

A. SiPM arrays

The two types of SiPM arrays tested are the following: AdvanSiD Hybrid TD Array NUV-SiPM (16 channels, 4 mm x 4 mm active area per channel) and Hamamatsu S14161-6050HS-04 (16 channels, 6 mm x6 mm active area per channel), a picture of them can be observed in Fig. 1, and their main characteristics can be seen in Table I, respectively. The Photon Detection Efficiency (PDE) of the SiPMs with respect to the wavelength and the emission curves of the plastic and liquid scintillators are illustrated in Fig. 2. The values of the integrated PDE of each SiPM multiplied by the normalized emission spectrum, which represent the probability that a scintillation photon that impinges the active area of the SiPM is being converted into a measurable current by the SiPM, can be seen in Table II. It is visible that the PDE of the two SiPM arrays covers the wavelength emission range of both organic scintillators, and the best match is seen with the Hamamatsu SiPM and the emission peak of the liquid scintillator.

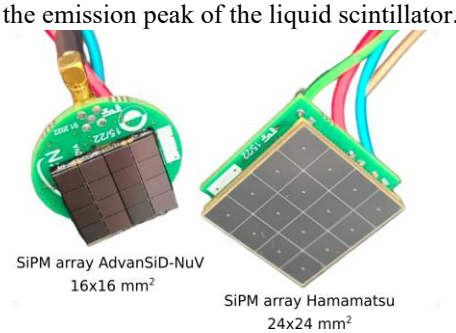

Fig. 1. Pictures of the AdvanSiD-NUV and Hamamatsu SiPM arrays.

Table I
Main characteristics of the SiPM arrays tested

	AdvanSiD-NUV	Hamamatsu
Array size	16.8 mm x 17.4 mm	25 mm x 25 mm
Single SiPM size	4 mm x 4 mm	6 mm x 6 mm
Channel number	16 channels	16 channels
No. of cells/channel	9340	14331
Cell size	40 µm x 40 µm	50 µm x 50 µm
Terminal capacitance Ct	90 fF	2000 pF
Peak sensitivity wavelength	420 nm (43%)	450 nm
Breakdown voltage, typ	26 V	38 V
Dark count rate @4V OV	< 100kHz/mm2	7.5 µA

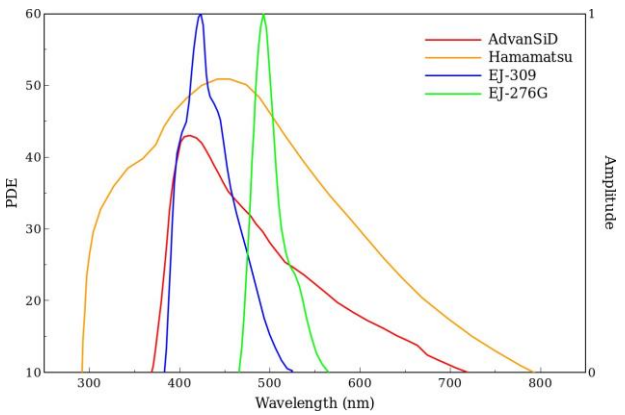

Fig. 2. Photon Detection Efficiency (PDE) corresponding to the AdvanSiD and Hamamatsu SiPM arrays (left axis) compared with the emission curves of the plastic and liquid scintillators (right axis). Information taken from the manufactures [5, 6, 11].

Table II
Integrated photon detection efficiency multiplied by the normalized emission spectrum for each SiPM array/scintillator combination

Detector + SiPM array	$\sum_{\lambda=250\,nm}^{900\,nm} \mathrm{PDE}(\lambda) \cdot \mathrm{I}(\lambda) \cdot \Delta\lambda$
EJ-276G + AdvanSiD	26.7
EJ-309 + AdvanSiD	36.6
EJ-276G + Hamamatsu	43.4
EJ-309 + Hamamatsu	48.4

B. Organic scintillators

In order to test the SiPM arrays, two organic scintillators with n/γ-ray discrimination capabilities were used, a plastic scintillator EJ-276G (25 mm dia. x 25 mm thick.) and a liquid scintillator EJ-309 (50 mm dia. x 50 mm thick.), both with cylindrical shape and from Eljen Technology–Texas USA. A small portion of optical grease was used for coupling the detectors to the SiPM arrays (see Fig. 3).

Fig. 3. Picture of the EJ-276G and the EJ-309 scintillators coupled to the AdvanSiD-NUV and Hamamatsu SiPM arrays, respectively.

C. Readout board of the SiPM arrays

The readout of the SiPM array output, and the bias voltage supply, was performed using a dedicated board, which follows the sequence, of four sets, where each set is made up of four single SiPMs connected in parallel. The output signals of each set are amplified using four trans-impedance preamplifiers based on an ultra-low noise, high-speed OpAmp (LMH6629). Then, the four amplified signals are summed giving the total output. For a better comprehension of the circuit a simple diagram of the readout board is shown in Fig. 4. Voltages of +/- 2.9 V are applied to each OpAmp. The applied bias voltage is between 30 and 40 V (depending on the SiPM array used). The same bias voltage is applied to each single SiPM.

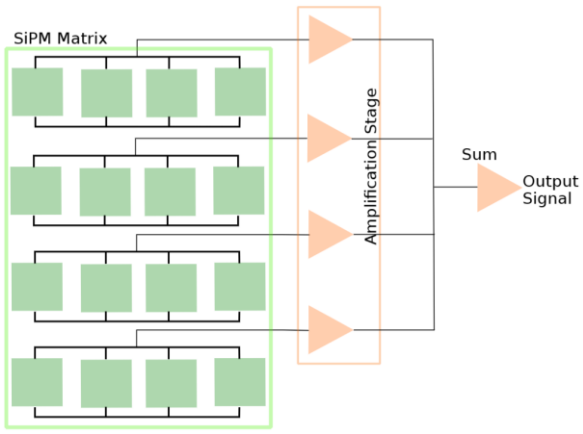

Fig. 4. Circuit diagram of the SiPM arrays' readout board.

D. Experimental details

The readout boards of the SiPM arrays were powered with an MT180T power supply. The overvoltage (OV) applied to each single SiPM was determined by optimizing the energy resolution corresponding to each assembled detector. The bias voltage (+800 V) applied to the $LaBr_3$:Ce detector, that is used for coincidence purposes, was delivered by a V6533 CAEN power supply unit controlled through a USB Controller (CAEN V1718). The output signals were digitized by a V1730 CAEN digitizer, which has a sampling rate of 500 MSamples/s, and an ADC resolution of 14-bit. Modern digitizers are based on a programmable FPGA (Field Programmable Gate Array), where the digitized waveform can be pre-processed online, the algorithm implemented in the digitizer provided for each triggered event, among others, the timestamp, and the total (Q_{total}) and partial (Q_{short}) integrals of the waveforms. Also, it is possible to acquire the digitized waveforms and analyze the data offline. Optical fiber connection was used to control the data acquisition. The digitizer was connected to the PC using a CAEN A4818 USB 3.0 to CONET2 Adapter. The ABCD (Acquisition and Broadcast of Collected Data) software [12, 13], which is provided as an open-source project (https://github.com/ec-jrc/abcd), was used to handle all aspects of the electronics and data acquisition. The following sources were used for the measurements: two γ-ray sources ^{22}Na and ^{137}Cs (~ 300 kBq), and one n/γ-ray source Am-Be (neutron emission rate ~ 2×105 s^{-1}).

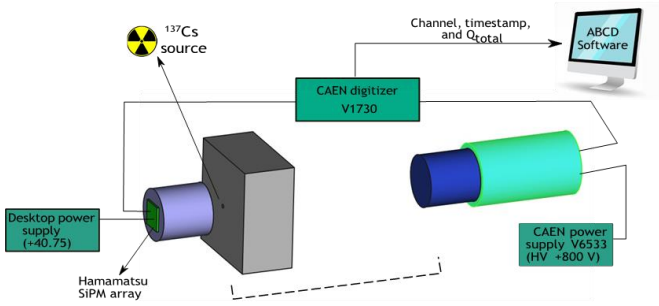

Fig. 5. Schematic view of the experimental setup used for the determination of the energy and time resolution, using the Hamamatsu SiPM array coupled to the EJ-309 detector in coincidence with the LaBr3:Ce detector, and placing the source and the collimator between both detectors. The electronic components used for data acquisition and high voltage supply are also displayed.

E. Determination of the energy and time resolution

The determination of the energy resolution of each assembled detector was conducted using a Compton coincidence technique, the details can be found in [14]. The method consists in setting up the organic detector under study in coincidence with a reference detector. In this case, the reference detector is a $LaBr_3$:Ce detector (50 mm diam. x 50 mm thick., from Saint-Goban). It was placed in front of the organic scintillator (face-to-face) at ~ 20 cm. A lead collimator with a cuboid form (10x10x5 cm^3) was located between both detectors, with a diameter of aperture of ~ 1 cm. A ^{137}Cs source (with activity of ~ 300 kBq) was attached to the collimator's hole (on the side of the organic detector). A schematic view of the experimental setup can be seen in Fig. 5. The method takes advantage of the fact that a γ-ray coming from the source (661.7 keV) can undergo a scattering of 180° on

the active volume of the organic detector, depositing approx. 477.4 keV, and then, the back-scattered γ-ray goes through the collimator's hole, reaches the reference detector, and deposits all its energy (184.3 keV). Finally, the main idea is to build the energy spectrum of the events, recorded by the organic detector under study, which are in coincidence with the full-energy events corresponding to the back-scattered γ-rays detected by the LaBr detector. In this case, the organic detector spectrum mainly consists of the Compton edge events. Then, a gaussian fit is applied, and the energy resolution of the detector is obtained by $R_E = FWHM/E_o$, where E_o=477.4 keV.

For the time resolution determination, the same experimental setup was employed, but in this case a ^{22}Na source (with activity of ~ 300 kBq) was used. An off-line analysis (coincidence filter) was performed on the digitized waveforms coming from each detector, with the purpose to optimize the parameters (fraction and delay) of the Digital Constant Fraction Discrimination (DCFD), the parameters were optimized to obtain the best time resolution. The delay parameter was varied from 10 ns to 100 ns, and for the fraction parameter, three values were considered 25%, 50%, and 75%. Then, the final time spectrum is built by considering the events in the full-energy peak (@511 keV) of the LaBr detector, and the events with energies greater that 150 keV of the organic detector.

F. Determination of the Pulse Shape Discrimination (PSD) capabilities

The n/γ-ray discrimination capability of each assembled detector under study was determined. An Am-Be neutron source was used for this purpose. The double gate integration method was employed to perform the pulse shape discrimination. It consists in calculating the pulse shape parameter (PSP), defined as PSP=(Q_{long} - Q_{short})/Q_{long}, where Q_{short} is the integral over a short time window including the fast rise time region and part of the fastest decay component of the pulse, and the Q_{long} is the integral over a long gate, encompassing the majority of the pulse. By analyzing the PSP distribution, it is possible to compute the Figure of Merit (FoM), defined as FoM =$\Delta/(\delta_n + \delta_\gamma)$, where Δ represents the difference between the mean values of the neutron and γ-ray distributions, while δ_n and δ_γ represent the Full Width at Half Maximum (FWHM) of the neutron and γ-ray distributions, respectively. The short and long integration gates needed to be optimized, until finding the maximum value of the FoM, which represents the best results in terms of n/γ-ray discrimination. The FoM values given in this work were determined using only the events located in a light output range corresponding approximately to Compton edge of the gamma line emitted by the ^{137}Cs source.

III. Results and Analysis

A. Signals comparison of both SiPM arrays

As the first step, a comparison of the output signals coming from both SiPM arrays was performed, for this purpose a ^{137}Cs source was used, and both SiPM arrays were coupled to the EJ-276G detector. In Fig. 6 it can be seen the typical waveforms for both cases. The signals correspond to an event with an energy equal to the Compton edge of the γ-ray emitted by the ^{137}Cs source. From the shape of the waveforms, in both cases the rising time is quite similar, while the decay time is so much faster in the case of the AdvanSiD-NUV array. Behavior that depends on the recharge time constant of the SiPM micro cells, which is proportional to the capacitance of the micro cell, ~RC (see Table I), and this parameter describes how quickly the micro cells can be recovered after detecting a scintillation photon.

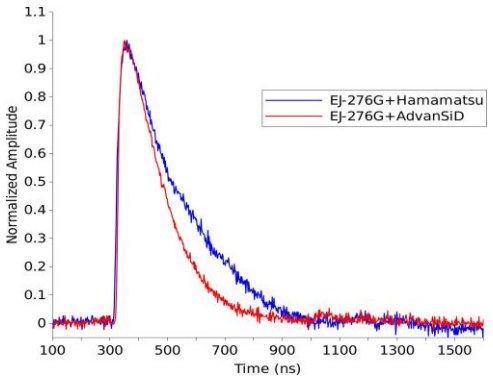

Fig. 6. Typical waveforms of the EJ-276G scintillator coupled to the Hamamatsu and AdvanSiD- NUV SiPM arrays. The signals correspond to an event of 477.4 keV, so the Compton edge of a 661.7 keV γ-ray.

B. Energy and Time Performance

The overvoltage applied to each scintillator/SiPM array configuration was optimized in function of the energy resolution, where the best performance was found for the voltages shown in Table III. The energy resolution determination was conducted using a Compton coincidence technique, as it was explained in Subsection 2.5. An illustration of the results obtained for one of the configurations can be seen in Fig. 7. Fig. 7a shows the energy spectrum of the LaBr detector in coincidence, wherein a red line series is seen as the energy selection corresponding to the back-scattered γ-ray full- energy peak at approx. 184.3 keV. Then, in Fig. 7b the energy spectrum of the EJ-309/Hamamatsu SiPM array assembly is shown, besides, the energy spectrum of the events that are in coincidence with the full-energy events of the back-scattered γ- rays are delineated with a green line. To get the energy resolution at 477.4 keV, the last-mentioned spectrum was fitted with a Gaussian function. Finally, using the set-up described in Subsection 2.5, the time spectrum obtained with the coincidences between the two γ-rays of 511 keV emitted by the ^{22}Na source is given in Fig. 7c.

TABLE III
BIAS VOLTAGE APPLIED TO EACH SCINTILLATOR/SIPM ARRAY CONFIGURATION

Scintillator/SiPM array	OV (V)
EJ-276G/AdvanSiD	4
EJ-276G/Hamamatsu	2.75
EJ-309/AdvanSiD	3.5
EJ-309/Hamamatsu	2.75

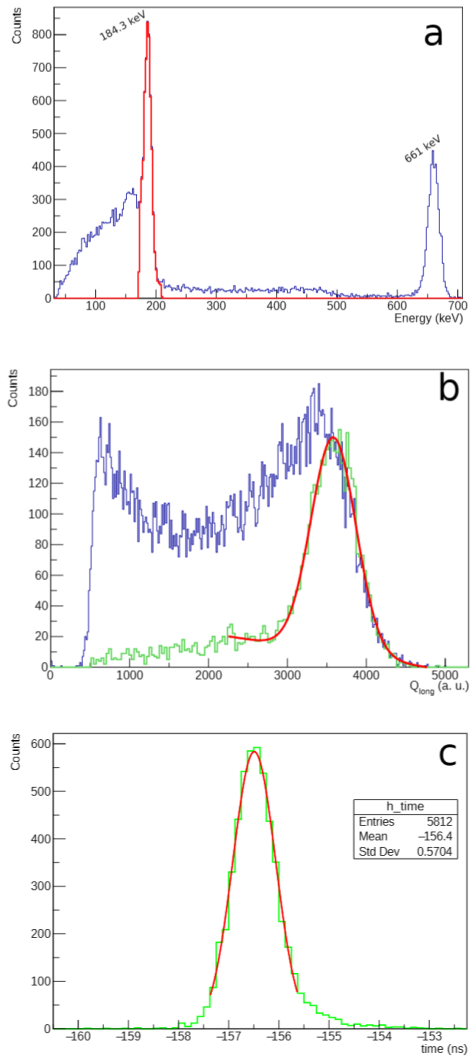

Fig. 7 (a) Energy spectrum of the LaBr detector in coincidence using the 137Cs source, wherein a red line it is shown the energy selection corresponding to the back-scattered γ-ray full-energy peak at approx. 184.3 keV. (b) Energy spectrum of the EJ-309/Hamamatsu SiPM array assembly in coincidence using the 137Cs, in green line the events that are in coincidence with the full-energy events of the back-scattered γ- rays. (c) Time spectrum of the coincidence experiment using the same detectors and the 22Na source.

On the other hand, for the time resolution determination, an offline analysis of the waveforms was carried out, where the DCFD's parameters were optimized in order to get the best time resolution. The optimal results were found using 120 ns of delay and 50% of fraction for the organic detectors/SiPM arrays assemblies, and 20 ns of delay and 20% of fraction for the LaBr detector. Then, another filter was implemented, by selecting the energy ranges of interest in each detector's spectrum, which corresponds to the 511 keV peak for the LaBr and all events with energies greater than 150 keV for the organic detector. A Gaussian fit is performed to the time spectrum, where the total time resolution (FWHM) of the system is obtained. The total time resolution corresponds to the following expression: $FWHM^2_{total} = FWHM^2_{LaBr} + FWHM^2_{Scintillator/SiPM}$, where the time resolution of the LaBr detector is 0.366±0.002, and in this way, the time resolution of the organic detector/SiPM array can be easily obtained. The same procedure for determining time and energy resolution was used for each organic scintillator/SiPM array assembly.

The results obtained can be seen in Table IV and Fig. 9. Despite the pulse's decay time of the AdvaSiD is faster than in the case of the Hamamatsu SiPM array (mentioned in Subsection 3.1), the Hamamatsu SiPM performances better in terms of energy and time resolution, for both organic scintillators. In particular, with the plastic scintillator, where the energy resolution of the Hamamatsu improved by 35% with respect to the AdvanSiD, and the time resolution improved by 40%.

TABLE IV
VALUES OF THE ENERGY AND TIME RESOLUTION OBTAINED FOR EACH SCINTILLATOR/SIPM ARRAY CONFIGURATION

Scintillator/ SiPM array	ENERGY RESOLUTION	TIME RESOLUTION (NS)
EJ-276G/ AdvanSiD-NUV	0.290 ± 0.002	1.84 ± 0.01
EJ-276G/ Hamamatsu	0.188±0.004	1.09 ± 0.01
EJ-309/ AdvanSiD-NUV	0.20 ± 0.02	1.30 ± 0.01
EJ-309/ Hamamatsu	0.108 ± 0.004	0.599± 0.004

C. *Neutron/γ-ray discrimination capability*

The discrimination capability of each combination scintillator/SiPM array was explored, using an Am-Be source and the double integration method. First, for each assembly, an optimization of the short and long integration gates was conducted, until finding the maximum value of the FoM. For each configuration, a 2D-PSP and PSP plots were obtained. The 2D-PSP plot corresponds to 2D histogram of the PSP values against the Q_{long} (it is proportional to the total light output) values. The PSP distribution plot is built with all the events that are in a light output range corresponding to the Compton edge associated to the γ-ray of 661.7 keV (^{137}Cs emission). The FoM value is calculated by analyzing the PSP distribution, as it was explained in Subsection 2.6. Fig. 8 shows the 2D-PSP and the PSP plots of the EJ-276G coupled to the Hamamatsu SiPM array, using an Am-Be source. In the 2D-PSP plot is highlighted in red the range of the events used for the construction of the PSP distribution. The FoM and the optimized values of the w_{long}, and the w_{short}, for each configuration can be seen in Table V. The FoM values of the Hamamatsu configuration outperform the AdvanSiD-NUV results by 43% with the liquid scintillator and 56% with the plastic scintillator.

TABLE V
OPTIMIZED INTEGRATION WINDOWS (W_{LONG} AND W_{SHORT}), AND FOM VALUES OBTAINED FOR EACH SCINTILLATOR/SIPM ARRAY CONFIGURATION

Scintillator/SiPM array	w_{long}	w_{short}	FoM
EJ-276G/AdvanSiD-NUV	904	240	0.76 ± 0.02
EJ-276G/Hamamatsu	590	220	1.19 ± 0.02
EJ-309/AdvanSiD-NUV	586	122	1.15 ± 0.01
EJ-309/Hamamatsu	730	180	2.04 ± 0.01

In Fig. 9 it can be seen an illustration of all the results obtained in this work, where it is notable the higher performance of the Hamamatsu SiPM array, in terms of energy resolution, time resolution, and discrimination capabilities. In particular, the best results were obtained with the EJ-309/Hamamatsu SiPM array assembly. The superior performance of the Hamamatsu SiPM array can be explained by several factors: The array size is bigger with respect to the AdvanSiD's area (see Table I), thus more light of each event can be collected. The Hamamatsu array covers the whole face of the plastic scintillator and ∼28% of the liquid's face area, while the AdvanSiD covers ∼60% and ∼15% respectively. Higher PDE (Photon Detection Efficiency), then the higher signal-to-noise ratio. And good matching between the PDE of the Hamamatsu SiPM and the emission spectrum of the detectors (see Table I and Fig. 2), increasing in that way the probability of detection.

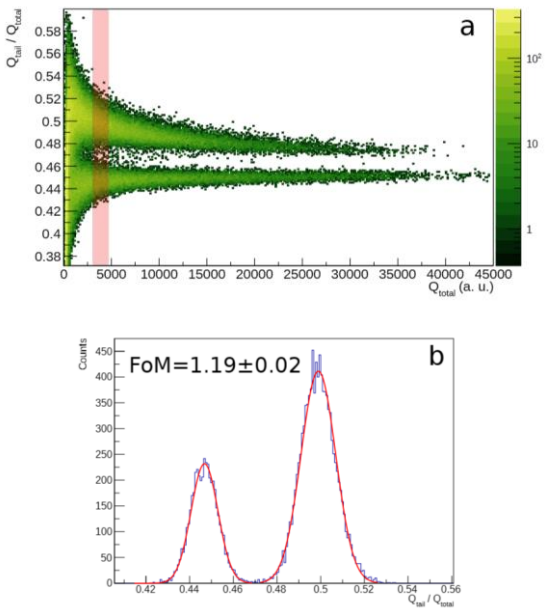

Fig. 8. 2D-PSP (a) and PSP (b) plots corresponding to the EJ-276G coupled to the Hamamatsu SiPM array, using an Am-Be source. In the 2D-PSP plot it is highlighted in red the range of the events used for the construction of the PSP distribution.

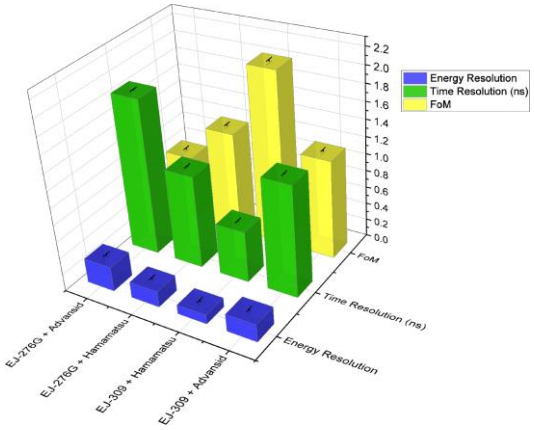

Fig. 9. Energy resolution, time resolution and FoM values of the EJ-309 and EJ-276G scintillators coupled to the AdvanSiD-NUV and Hamamatsu SiPM arrays.

IV. CONCLUSIONS

In this paper, two types of SiPM array sensors were compared in terms of energy resolution, time resolution, and discrimination capabilities between neutrons and γ-rays. Specifically, the SiPM arrays investigated are the AdvanSiD hybrid array ASD- NUV4S-P-4x4TD 17 mm x17 mm and the MPPC Hamamatsu S14161-6050HS-04 25 mm x 25 mm. To conduct the tests, we coupled the SiPM arrays to two organic scintillators that possess n/γ-rays discrimination capabilities, a plastic scintillator EJ-276G (25 mm dia. x 25 mm thick) and a liquid scintillator EJ-309 (50 mm dia. x 50 mm thick), both from Eljen Technology, Texas USA. Our objective is to provide a detailed performance analysis of these four configurations, considering that by studying the performance characteristics of SiPMs, researchers can gain a better understanding of their capabilities and limitations. Furthermore, as SiPMs are becoming increasingly popular in research and industry, it is important to have a thorough understanding of their properties in order to make informed decisions regarding their selection and use. To determine the energy and time resolution, a coincidence experiment was conducted, using a LaBr detector. For the energy resolution determination, a Compton coincidence technique was applied, where the energy resolution of each configuration was obtained at 477.4 keV, which represents the energy deposited of a γ-ray of 661.7 keV (coming from a 137Cs source) after suffering a back-scattering interaction in the active volume of the detector. From all the configurations studied, the EJ-309/Hamamatsu SiPM array gave the best performance, with an energy resolution of ∼10%, and with a time resolution of (0.599±0.004) ns, overcoming the results of the AdvanSiD-NUV array (using the same scintillator), where the values of energy resolution and the time resolution increased by 46% and 53%, respectively. Also, the bias voltage applied to the arrays was optimized in function of the energy resolution. For the determination of the time resolution, a 22Na source was used, where the annihilation 511 keV γ-rays were measured in both detectors (the organic and the LaBr).

On the other hand, the study of the discrimination capability consisted in using a mixed n/γ-ray source (AmBe source), where the performance of the SiPM arrays coupled to the

organic detectors is compared in function of the FoM value, which is a quantitative measure used to evaluate the discrimination capability of a system. Once more, the Hamamatsu SiPM array with the EJ-309 liquid scintillator showed a superior performance, giving a FoM value of 2.04, 43% greater than the AdvanSiD-NUV array. From the results obtained in this work, it has been concluded that the Hamamatsu SiPM array performs better than the AdvanSiD-NUV due to its larger array size, greater Photon Detection Efficiency, higher signal-to-noise ratio, and good matching with the emission spectrum of the scintillators.

REFERENCES

[1] "Introduction to silicon photomultipliers (SiPMs)," First Sensor, Tech. Rep., 2019.
[2] E. Garutti, "Silicon photomultipliers for high energy physics detectors," Journal of Instrumentation, vol. 6, no. 10, pp. C10 003–C10 003, Oct. 2011.
[3] R. M. Preston, J. E. Eberhardt, and J. R. Tickner, "Neutron-Gamma Pulse Shape Discrimination Using Organic Scintillators with Silicon Photomultiplier Readout," IEEE Transactions on Nuclear Science, vol. 61, no. 4, pp. 2410–2418, Aug. 2014.
[4] "Introduction to SiPM. technical note," SensL, Tech. Rep., 2017.
[5] "MPPCs (SiPMs) / SPADs | Hamamatsu Photonics." [Online]. Available: https://www.hamamatsu.com/eu/en/product/optical-sensors/mppc.html
[6] "Products." [Online]. Available: https://www.broadcom.com/products. Accessed on: April 15, 2023.
[7] F. Pino, J. Delgado, G. Mantovani, L. Pancheri, M. Bello, D. Fabris, C. L. Fontana, M. Polo, V. Ruiz, D. Brunelli, A. Quaranta, and S. Moretto, "Novel Detector Assembly for Neutron/Gamma-Ray Discrimination Applications Based on Large- Sized Scintillators Coupled to Large Area SiPM Arrays," IEEE Transactions on Nuclear Science, vol. 69, no. 4, pp. 668–676, Apr. 2022.
[8] M. Grodzicka-Kobylka, T. Szczesniak, and M. Moszyn´ski, "Comparison of SensL and Hamamatsu 4×4 channel SiPM arrays in gamma spectrometry with scintillators," Nuclear Instruments and Methods in Physics Research Section A: Accelerators, Spectrometers, Detectors and Associated Equipment, vol. 856, pp. 53–64, Jun. 2017. [Online]. Available: https://linkinghub.elsevier.com/retrieve/pii/S0168900217303388. Accessed on: April 15, 2023.
[9] F. Pino, C. Fontana, J. Delgado, D. Fabris, G. Nebbia, M. Turcato, D. Brunelli, L. Pancheri, A. Quaranta, and S. Moretto, "Characterization of a medium-sized CLLB scintillator: single neutron/gamma detector for radiation monitoring," Journal of Instrumentation, vol. 16, no. 11, p. P11034, Nov. 2021. [Online]. Available: https://iopscience.iop.org/article/10.1088/1748-0221/16/11/P11034. Accessed on: April 15, 2023.
[10] D. Cester, G. Nebbia, L. Stevanato, F. Pino, L. Sajo-Bohus, and G. Viesti, "A compact neutron–gamma spectrometer," Nuclear Instruments and Methods in Physics Research Section A: Accelerators, Spectrometers, Detectors and Associated Equipment, vol. 719, pp. 81–84, Aug. 2013. [Online]. Available: https://linkinghub.elsevier.com/retrieve/pii/S0168900213004373. Accessed on: April 15, 2023.
[11] "Products - Eljen Technology." [Online]. Available: https://eljentechnology.com/products. Accessed on: April 15, 2023.
[12] C. L. Fontana, M. Lunardon, F. E. Pino, L. Stevanato, A. Carnera, C. Sada, F. Soramel, and S. Moretto, "A distributed data acquisition system for signal digitizers with on-line analysis capabilities," in 2017 IEEE Nuclear Science Sym- posium and Medical Imaging Conference (NSS/MIC). Atlanta, GA: IEEE, Oct. 2017, pp. 1–5. [Online]. Available: https://ieeexplore.ieee.org/document/8533063/. Accessed on: April 15, 2023.
[13] C. L. Fontana, A. Carnera, M. Lunardon, F. E. Pino, C. Sada, F. So- ramel, L. Stevanato, and S. Moretto, "A distributed data acquisition system for nuclear detectors," International Journal of Modern Physics: Conference Series, vol. 48, p. 1860118, Jan. 2018. [Online]. Available: https://www.worldscientific.com/doi/abs/10.1142/S2010194518601187. Accessed on: April 15, 2023.
[14] L. Swiderski, M. Moszynski, W. Czarnacki, J. Iwanowska, A. Syntfeld Kazuch, T. Szczesniak, G. Pausch, C. Plettner, and K. Roemer, "Measurement of Compton edge position in low-Z scintillators," Radiation Measurements, vol. 45, no. 3-6, pp. 605–607, Mar. 2010. [Online]. Available: https://linkinghub.elsevier.com/retrieve/pii/S1350448709001917. Accessed on: April 15, 2023.